Adaptive coding across visual features during free-viewing and fixation conditions

Sunny Nigam[1*], Russell Milton[1], Sorin Pojoga[1], Valentin Dragoi[1,2*]

[1]Department of Neurobiology & Anatomy
McGovern Medical School, University of Texas at Houston
Houston, TX 77030

[2]Department of Electrical and Computer Engineering
Rice University
Houston, TX 77005

[*] Correspondence to: sunny.nigam@uth.tmc.edu; valentin.dragoi@uth.tmc.edu

ABSTRACT

Theoretical studies have long proposed that adaptation allows the brain to effectively use the limited response range of sensory neurons to encode widely varying natural inputs. However, despite this influential view, experimental studies have exclusively focused on how the neural code adapts to a range of stimuli lying along a single feature axis, such as orientation or contrast. Here, we performed electrical recordings in macaque visual cortex (area V4) to reveal significant adaptive changes in the neural code of single cells and populations across multiple feature axes. Both during free viewing and passive fixation, populations of cells improved their ability to encode image features after rapid exposure to stimuli lying on orthogonal feature axes even in the absence of initial tuning to these stimuli. These results reveal a remarkable adaptive capacity of visual cortical populations to improve network computations relevant for natural viewing despite the modularity of the functional cortical architecture.

Introduction

One influential view in neuroscience is that sensory cortical neurons are adapted to the statistics of natural stimuli[1–3]. According to this view, adaptation allows sensory neurons to make effective use of the limited range of neural responses to encode stimuli that vary widely in structure, such as those encountered in natural environments[4]. During visual perception, for instance, the exploration of natural scenes consists of successive visual fixations accompanied by changes in image statistics[5,6]. However, natural images, despite their complexity, have certain common statistical properties. That is, neighboring image patches are highly correlated in local attributes, such as orientation, contrast, or color, whereas distant image patches are only poorly correlated[7,8]. Therefore, successive fixations during natural viewing will often land on image patches of largely different structure. Orientation and color signals, two of the elementary features ubiquitously present in natural scenes, are considered to be orthogonal to each other as they are represented in distinct modules in primate mid-level visual cortex[9,10]. It is conceivable that during a typical visual fixation, neurons can be exposed to image patches dominated by oriented signals, while subsequent fixations could land on distant image patches where color is the primary feature (Fig. 1a, Supplementary Fig. 1). However, although successive fixations to orthogonal image features are ubiquitous during natural viewing (Fig. 1a), whether and how cross-feature adaptation influences neuronal responses and stimulus coding remains unknown.

Previous adaptation studies have shown that rapid exposure to spatially correlated image patches induces short-term changes in the responses of visual cortical neurons and changes the tuning of individual cells and their stimulus discriminability[6,11]. At the population level, rapid adaptation was shown to reduce neuronal correlations and improve coding accuracy[12,13]. However, while these results were instrumental for our current understanding of the properties of the adaptive code, they originated from studies investigating how the neural code adapts to a relatively narrow set of stimuli along a single feature axis, such as orientation[14,15], contrast[16,17], motion[18,19] or color[20]. Equally important, previous adaptation studies have exclusively focused on experimental paradigms involving restricted viewing in which stimuli are presented during passive fixation, thereby lacking the naturalistic conditions encountered during free-viewing.

Here, we addressed two of the major limitations of previous adaptation studies by simultaneously recording the spiking activity of multiple neurons from superficial layers of visual cortical area V4 of awake macaque using chronically implanted Utah arrays (Fig. 1c, d). While monkeys freely viewed or fixated on stimuli of largely dissimilar structure, we examined whether successive fixations to image patches across orthogonal feature axes induce adaptive changes in the properties of the neural code.

Results

The efficient coding hypothesis[1] predicates that visual cortical responses are adapted to the statistics of natural stimuli during vision. That is, the higher the frequency of particular stimuli encountered during natural vision, the more efficient the neural mechanisms responsible for processing those stimuli. In light of this hypothesis, we examined how likely successive fixations occurring during natural viewing could land on cross-feature stimuli (considering that each fixation episode would act as rapid adaptation[6]). To this end, we built a statistical model of visual exploration of natural scenes to examine the features encountered in consecutive fixations. We

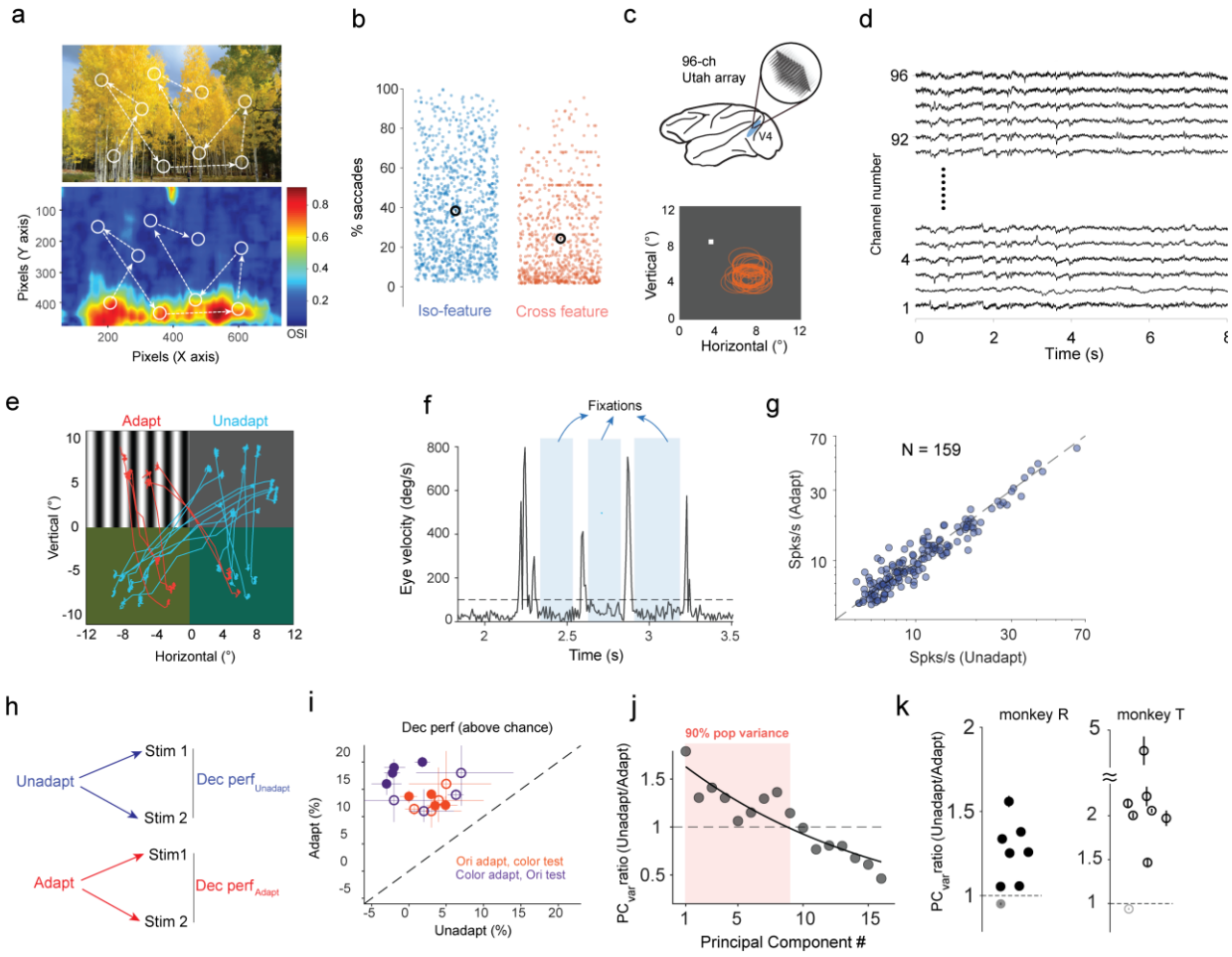

Fig. 1 Rapid adaptation during free-viewing improves coding accuracy in neural populations. a Top: Natural scene showing simulated saccades with circles and dotted arrows representing pseudo receptive fields and direction of saccades respectively. Bottom: Heatmap of orientation selectivity index (OSI) calculated on the same image using a Sobel filter on patches of size 50 x 50 pixels sliding by 10 pixels along x/y directions. Simulated saccades generated in top panel have been overlaid to depict how orientation signals change within RFs due to saccades. b Percentage of simulated saccades connecting patches with similar (iso-feature, light blue dots) and dissimilar features (cross-feature, orange dots). Individual dots represent the mean percentage of saccades calculated for each natural image used in the analysis. Black unfilled circles and vertical bars represent mean and s.e.m of the distributions. **c** Top: Schematic description of a chronically implanted 96 channel Utah array in macaque visual area V4. Bottom: Position of receptive fields (RF, orange circles) of single units analyzed with respect to fixation point (white dot). **d** Snippet of voltage waveforms recorded simultaneously from all 96 channels. **e** Stimulus configuration for free-viewing experiments (examples of successive fixations). Red and blue traces show saccades connecting the center mass of the receptive fields during fixations in 'adapt' and 'unadapt' conditions. **f** Representative example of fixation detection from eye velocity trace during free-viewing using velocity thresholding (see Methods). Blue shaded regions represent fixation periods. **g** Firing rates for individual neurons (N = 159) during fixations detected while free-viewing across 16 sessions for unadapted and adapted conditions (mean values: FR_{adapt} = 11.8 Hz, $FR_{unadapt}$ = 12.1 Hz; Wilcoxon signed rank test, P > 0.05). **h** Schematic describing decoder performance of distinguishing between 2 test stimuli under unadapt (blue) and adapt conditions (red). **i** Decoder performance (chance level subtracted) for unadapted and adapted conditions in case of an orientation adapter and color test stimuli (orange) and color adapter and orientation test stimuli (purple). Filled and open circles represent individual sessions from monkey T and R respectively. Vertical and horizontal error bars represent s.e.m calculated over 500 iterations of the classifier in each condition. **j** Ratio of the population variance captured in trial-by-trial responses by principal components (PCs) in unadapt and adapt conditions for an example session. Adapted responses are projected onto the principal component axis derived from unadapt condition. Shaded orange patch denotes the number of PCs that capture 90% of the population variance across trials in the unadapted condition. Filled gray circles represent the ratio along each PC axis and solid black line represents an exponential fit (for visualization purposes). **k** Mean value of the ratio of population variance explained by principal components that account for 90% of the variance for each

individual session in monkey R (solid black circles) and monkey T (open black circles). Error bars were evaluated by performing PCA analysis on sub-sampled trials in each condition. Lighter shaded circles represent sessions where the ratio is not significantly greater than 1 (Wilcoxon signed rank test, $P > 0.05$).

focused on quantifying the distribution of visual fixations on two elementary features that are ubiquitously present in natural scenes: color and orientation. Based on the distribution of saccade amplitude and direction while monkeys are freely viewing a visual display across 16 sessions (Fig. 1e and Supplementary Fig. 2, see Methods), we simulated consecutive pseudo-saccades by using a natural image battery (n = 940) from the McGill calibrated color image data base (McGill Vision research). For each image we randomly assigned a fixation starting point, and then generated 300 consecutive saccades (we analyzed a total of 282,000 saccades across the images from the data base). The size of image patches was chosen based on mean receptive field size of our V4 neurons. For every pseudo saccade connecting two patches of the natural image, we quantified the strength of orientation and color signals in each patch (see Methods). Strikingly, we found that a significant percentage of saccades (23%) involved successively fixated image patches characterized by dissimilar features (color → orientation and orientation → color) at the start and end points (Fig. 1b). This analysis indicates that during the visual exploration of natural images, visual cortical neurons are highly likely to be exposed to successive image patches containing dissimilar visual features (orientation and color).

Given the ubiquity of exposure to largely different features during viewing natural stimuli, we designed a naturalistic task (Fig. 1e), where monkeys freely viewed four stimuli placed on different quadrants of a visual display. The top right quadrant contained a uniform gray patch (control stimulus), whereas the top left quadrant contained an adapting stimulus (achromatic grating or color patch). The bottom two quadrants contained two test stimuli separated by 22.5° in u.v. color space (when grating adapters were used; see Methods) or by 11.25° in orientation space (when color adapters were used). The receptive fields of multiple neurons recorded simultaneously were mapped at the beginning of each recording session (Fig. 1c bottom, see Methods). The adapter and test stimuli were chosen to maximize the number of responsive units on a given session. Control trials were defined as fixations on the gray patch followed by fixations on a test stimulus in either quadrant, whereas adaptation trials consisted of fixations on the adapter patch (grating or color) followed by fixations on either of the test stimuli (Fig. 1e). Fixations were detected during free viewing by thresholding eye velocity (Fig. 1f; see Methods). Only fixations whereby neurons' aggregate receptive fields were confined within the monitor borders and within a single quadrant, were considered for further analysis. We analyzed the responses of 159 single units (mean firing rate > 5 Hz for both unadapted and adapted conditions) in 2 monkeys (T and R) during 9,835 fixations recorded from 21.2 hours of free viewing across 16 sessions (8 sessions from each animal).

Improved population coding accuracy during free-viewing

We examined the extent to which the neural population can distinguish between pairs of test stimuli in control and adaptation trials during free viewing given that there was no significant difference in the mean responses of single neurons (Fig. 1g, Wilcoxon signed rank test, $P>0.05$). To this end, we pooled neurons' responses during fixations to each test stimulus when they were preceded by the gray (control) patch or the oriented grating adapter. To examine whether cross-feature adaptation influences stimulus coding (Fig. 1h), we calculated spike counts during fixations on each test stimuli in either condition (unadapt/adapt), and then implemented a linear decoder (Linear Discriminant Analysis; see Methods). Notably, we observed an increase in decoder

performance (DP) for color stimuli when cells were adapted to a different feature, i.e., orientation, and vice-versa when color was the adapter and orientation was used for test stimuli (Fig. 1i; $\Delta DP_{adapt\_ori} = 19 \pm 2\%$; $\Delta DP_{adapt\_color} = 30 \pm 4\%$, mean ± s.e.m). These results are surprising given that orientation and color are assumed to be encoded independently in visual cortex given their modular functional organization.

To understand how cross-feature adaptation leads to improved stimulus discriminability, we analyzed the structure of trial-by-trial responses of the entire neural population in the unadapted and adapted conditions (see Supplementary Fig. 3a for a pairwise correlation analysis). We hypothesized that decoder performance in the adapted condition is improved because the population response is more decorrelated, i.e., the shared variability between neurons is reduced. To examine this, we performed a principal component analysis on the responses of neurons across trials[21,22] in the unadapted condition. Next, we projected the activity of the same neurons in the adapted condition onto the principal component axis obtained in the unadapted condition. To quantify the changes in the overall structure of shared population wide variability, we calculated the ratio of the variance explained along each principal component axis in unadapted and adapted conditions (Fig. 1j, example session 5). Finally, we calculated the mean value of the ratios for the principal components that explained 90% of the variance in the control condition. Interestingly, we found a significant reduction in explained variance (along the same PC axis) post adaptation in the vast majority of sessions in both animals (Fig. 1k, Wilcoxon signed rank test, $P < 0.01$). A similar decrease in explained variance across conditions is found even if we consider only the first PC axis (Supplementary Fig. 3b) indicating that our analysis is robust to the number of principal components chosen. Thus, our analysis shows that in the higher dimensional space of neural responses there is a transition from an ellipsoid to a more spherical clustering of neuronal responses post adaptation indicating an overall decorrelation of the population response, which may be the likely mechanism for the improvement in decoder accuracy.

One possible confound is the duration of fixations on the adapter preceding each test stimulus. A mean duration of fixations on the adapter preceding $test_1$ that is different from that of fixations preceding $test_2$ is equivalent to different strengths of adaptation that could conflate the interpretation of the decoder results in Fig. 1i. However, we found no significant difference between the fixation durations preceding each test stimulus ($P > 0.01$; Wilcoxon's rank-sum test; Supplementary Fig. 4a). We further analyzed other factors that could possibly account for the changes in decoder performance not directly linked to rapid adaptation. However, there were no significant differences in the distribution of fixation durations on the post-adaptation test stimuli, mean pupil size, subthreshold eye velocity of microsaccades during fixations, number and direction of microsaccades between unadapted and adapted conditions ($P > 0.05$ for all comparisons, Wilcoxon rank sum test, Supplementary Fig. 4b-e). We observed no systematic changes in the mean firing rates of neurons associated with direction of saccades to different test stimuli (Wilcoxon signed rank test, $P > 0.1$). Additionally, the average distance between the neurons' receptive fields centers and the boundary between the two test stimuli did not differ significantly between adapted and unadapted conditions ($P>0.05$, Wilcoxon rank sum test; Supplementary Fig. 4f). Altogether, these analyses indicate that the changes in decoder performance after rapid adaptation during natural viewing cannot be attributed to confounding factors related to eye movements or our experimental design.

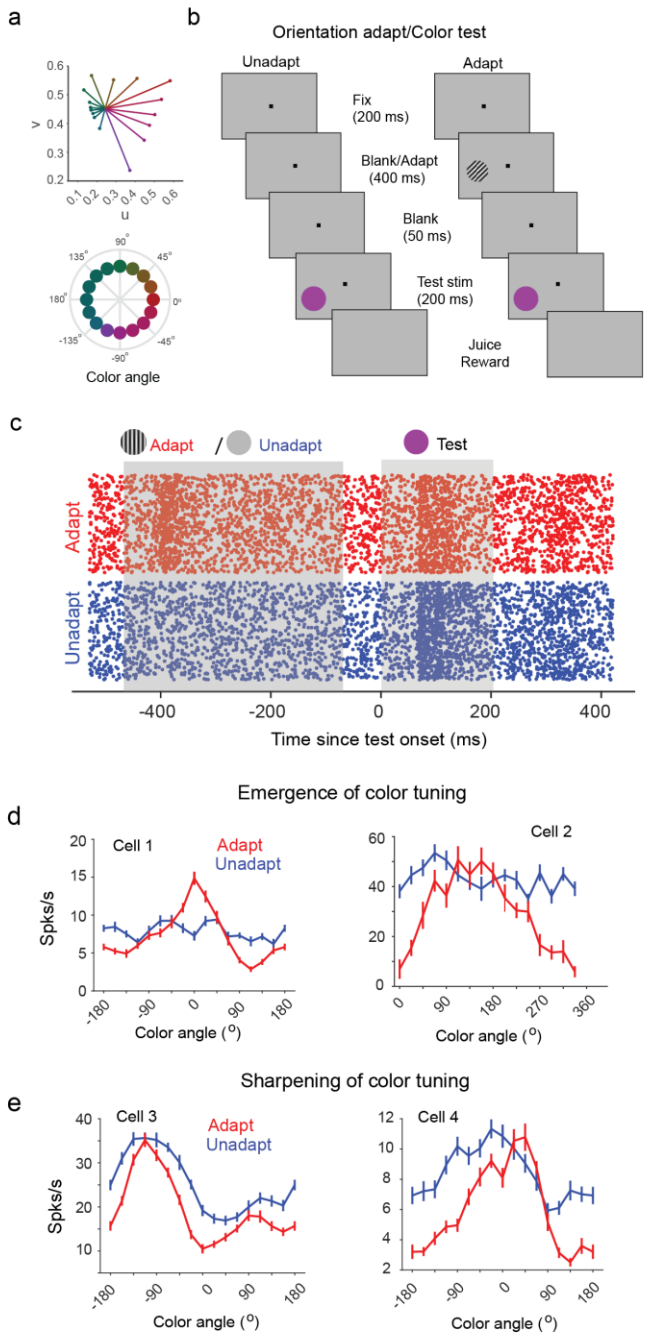

Emergence of feature tuning after adaptation to the orthogonal feature

While the free viewing task allowed us to investigate cross-feature adaptation effects under naturalistic conditions, the experimental design limited us to studying stimulus coding using only one pair of test stimuli. Therefore, to examine how cross-feature adaptation impacts overall tuning properties, such as strength of tuning and stimulus preference, we performed additional experiments involving passive visual fixation. Stimulus tuning was measured using an extended set of oriented gratings and color patches while recording the visually driven spiking activity of hundreds of neurons (n = 523) from the superficial layers of V4 (10 sessions in monkey T; 7 sessions in monkey M). Stimuli consisted of color patches and oriented gratings used either as adapters or test stimuli. Responses to color stimuli were quantified using a set of 16 equiluminant colors (9.35 ± 0.01 cd/m^2) uniformly spaced in Luv color space (steps of 22.5º) with respect to a neutral gray point [20] (Fig. 2a, Supplementary table 1; see Methods), while those to oriented stimuli were examined using 16 sinusoidal gratings uniformly spanning the 0°-180° range in steps of 11.25° (same mean luminance as the color patches and gray background). Using these stimuli, we characterized the tuning preference of neurons to find that 63.7% of the neurons were only tuned to color, 13.2% were only tuned to orientation, 8.8% were tuned to

Fig. 2 Emergence and enhancement of color tuning after adaptation to oriented stimuli. a Equiluminant color stimulus set plotted in *u*,*v* space. Angular plot of same color stimulus with respect to the *u*,*v* coordinates of an equiluminant neutral gray background on which adapter and test stimuli are presented. **b** Schematic description of the cross-feature adaptation task. Adapter and test stimuli are flashed across the receptive fields of recorded neurons. **c** Raster plot of an example neuron across multiple trials consisting of unadapted (blue) and adapted (red) conditions. Gray shaded regions represent the duration of the adapter (400 ms) and test stimulus (200 ms) presentation. **d** Tuning curves of example neurons showing emergence of color tuning in color untuned neurons (cell 1, monkey T, CSI_{adapt} = 0.26, $CSI_{unadapt}$ = 0.05; cell 2, monkey M, CSI_{adapt} = 0.24, $CSI_{unadapt}$ = 0.05) after adaptation with an oriented grating. **e** Tuning curves for color stimuli in two other example neurons (cell 3, monkey T, CSI_{adapt} = 0.21, $CSI_{unadapt}$ = 0.15; cell 4, monkey M, CSI_{adapt} = 0.30, $CSI_{unadapt}$ = 0.13) exhibiting sharpening of color tuning after orientation adaptation. Solid lines and error bars represent the mean and s.e.m of responses to color stimuli (see also Supplementary fig. 4).

both color and orientation, and 13.2% were not significantly tuned to either color or orientation. Each recording session consisted of randomly interleaved unadapted and adapted trials (n = 450 ± 30 trials/condition). During adaptation trials, a 400-ms adapting stimulus belonging to one feature set (e.g., orientation) was followed by a 200-ms stimulus randomly selected from the orthogonal feature set (color) with an inter-stimulus interval of 50 ms. Control (unadapted) trials did not contain an adapting stimulus; instead, a gray screen was presented for the same duration as that of the adapter (Fig. 2b-c).

Strikingly, many cells in our population either acquired color tuning or significantly sharpened it after orientation adaptation (Fig. 2d-e, see Supplementary Fig. 5 for additional examples). This is surprising since color and orientation were shown to be processed independently in anatomically non-overlapping modules in V4. Across sessions, we observed a small but significant decrease in peak firing rates (FR) after adaptation (Fig. 3a, Wilcoxon signed tank test, $P < 0.05$, $\Delta FR_{adapt\text{-}unadapt} = -3.3 \pm 1.4$ %, Fig. 3a inset). A significant proportion of color untuned neurons (18%) became significantly tuned ($P < 0.05$; Rayleigh's test; Holm-Bonferroni correction for multiple comparisons; Fig. 3b) after exposure to a fixed oriented grating (see Supplementary Fig. 6 for results in each animal). In addition, adaptation increased the strength of color tuning (Fig. 3b) in roughly 45% of V4 neurons (statistical significance and strength of color tuning were examined using Rayleigh's test and Color Selectivity Index, CSI, see Methods). Across the population of cells, we observed a net increase in the strength of color tuning strength after adaptation (Fig. 3b inset; $\Delta CSI_{adapt\text{-}unadapt} = 60 \pm 7\%$, $P < 0.001$, Wilcoxon signed rank test).

In general, we noticed that adapters that strongly activated neurons had a tendency to induce or enhance color tuning in neurons that were either untuned or weakly color tuned before adaptation (Fig. 3c, effective adapter). In contrast, adapters that only weakly activated neurons had a minimal impact on color tuning (Fig. 3d, ineffective adapter). Across the population, we found a significant correlation between how strongly an adapter activates the cell and the post-adaptation change in CSI (Fig. 3e; Spearman's correlation coefficient $r = 0.19$, $P = 0.0004$). Changes in tuning strength were also associated with changes in the temporal dynamics of color tuning. We calculated CSI as a function of time using a 200-ms window sliding by 5 ms, and defined tuning latency (TL) as the first time point when the neuron's tuning achieved statistical significance (Rayleigh's test). Tuning latency was significantly higher in the adapted compared to unadapted condition (Supplementary Fig. 7; Wilcoxon's signed-rank test, $P < 0.0001$, $\Delta TL_{adapt\text{-}unadapt} = 21.6 \pm 0.3$ ms). We found only modest changes in preferred color after adaptation ($\Delta\theta_{mean} = 1.4^{o}$, Supplementary Fig. 8).

Cross-feature adaptation improves population coding

Does cross-feature adaptation improve the ability of neuronal populations to discriminate between neighboring stimuli as observed in our free-viewing experiments? A classifier (linear discriminant analysis; see Methods) was trained to decode information from the responses of neural populations for neighboring color stimuli (separated by 22.5° on the color circle, Fig. 2a). Confirming our results in Fig. 1i, there was a significant increase in mean decoder accuracy after adaptation (Fig. 3f; mean $change_{adapt\text{-}unadapt} = 5 \pm 1\%$; $n = 17$ sessions, $N = 500$ iterations). This improved performance in decoding is surprising given the small, but significant decrease in overall firing

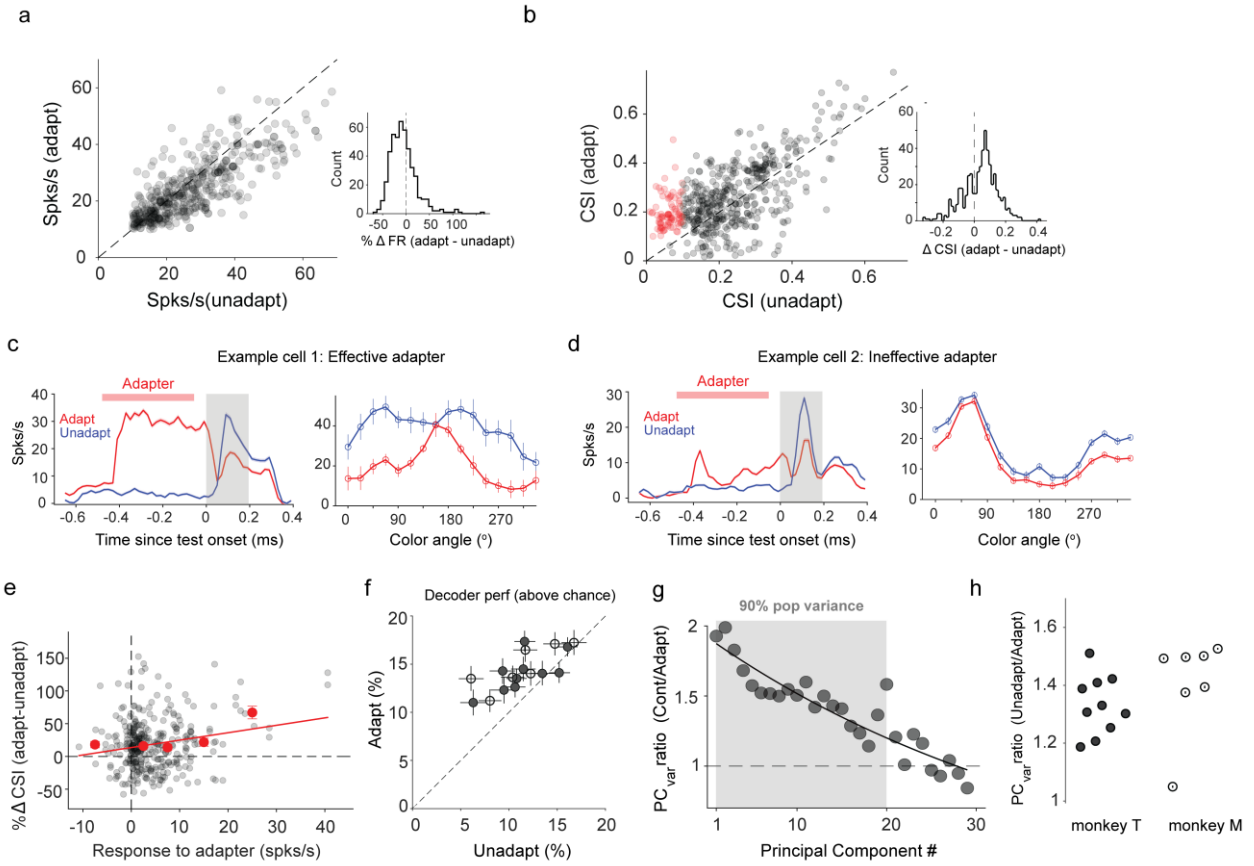

Figure 3. Cross feature adaptation modulates stimulus coding. a Mean peak responses of neurons (n = 388) to color stimuli for adapted and unadapted trials. Inset shows distribution of percent differences in responses (adapt – unadapt). **b** Color selectivity index (CSI) for neurons in adapted and unadapted conditions. Red circles represent neurons that were untuned to color in the unadapted condition but gained significant color tuning after orientation adaptation. Inset shows the distribution of change in CSI values (adapt – unadapt, $\Delta CSI_{mean} = 0.04$) calculated for all neurons. **c** Post stimulus time histogram (PSTH) averaged over adapted (red) and unadapted trials (blue) of an example neuron (left) strongly activated by an effective oriented adapter and its associated tuning curve under both conditions (right). Red bar and gray shaded region represent the duration of the adapter and test stimuli. **d** A different example cell showing weak activation by an ineffective adapter and associated tuning curves under both conditions. Solid lines and shaded regions represent mean values and s.e.m respectively. **e** Percentage change in CSI for neurons (n = 283) that were significantly tuned under both adapted and unadapted conditions as a function of the baseline corrected response to the adapter. Black circles represent individual neurons, solid red circles represent mean of binned values and error bars represent s.e.m. Solid red line represents a linear fit to the binned values. **f** Mean decoder accuracy (%) above chance for classifying neighboring color stimuli based on the response of the neuronal population in each session (gray filled circle, N = 10 sessions monkey T; black open circles, N = 7 sessions monkey M) in unadapted and adapted condition. Error bars represent s.e.m for decoder accuracy evaluated over multiple iterations of the classifier. **g** Ratio of the population variance captured in the trial-by-trial responses by principal components in unadapt and adapt conditions for an example session. Adapted responses are projected on to the principal component axis derived from unadapt condition. Shaded gray patch denotes the number of principal components that capture 90% of the population variance across trials in the unadapted condition. Filled gray circles represent the ratio along each PC axis and solid black line represents an exponential fit included for visualization purposes. **h** Mean value of the ratio of variance explained by principal components that account for 90% of the population variance for each individual session in monkey T (black filled circles) and monkey M (black open circles). Error bars were evaluated by performing PCA analysis multiple times on sub-sampled trials in each condition.

rates post adaptation (Fig. 3a). This indicates that rapid adaptation to one visual feature improves population coding accuracy to distinguish between stimuli lying on an orthogonal feature axis.

To verify whether a similar mechanism to that occurring during free-viewing could explain the post-adaptation improved decoder performance during passive fixation, we repeated the principal component analysis on neurons' responses during the unadapted and adapted conditions (Fig. 3g, example session). We observed a significant reduction in variance of neural activity along principal component axes in adapted compared to unadapted conditions (Fig. 3h), i.e., population level activity was more decorrelated after adaptation, similar to the effects observed during free-viewing. This was surprising given that both the mean and the variance of the distribution of pairwise correlations were not significantly altered after adaptation (Supplementary Fig. 9). These results are robust with respect to the number of PC axes used, as we observed similar trends by considering only the first principal component axis (Supplementary Fig. 10a). This suggests that the decorrelation of neural responses across the population could be a general mechanism by which cross feature adaptation improves stimulus discriminability in both free-viewing and passively fixating animals.

Cross-feature color adaptation

We further examined whether our results still hold when the adapting and test stimuli used in the experiments in Figs. 2-3, are swapped. Specifically, we analyzed neurons' responses to orientation after they were adapted to color while leaving all other task parameters unchanged (Fig. 4a; N=7

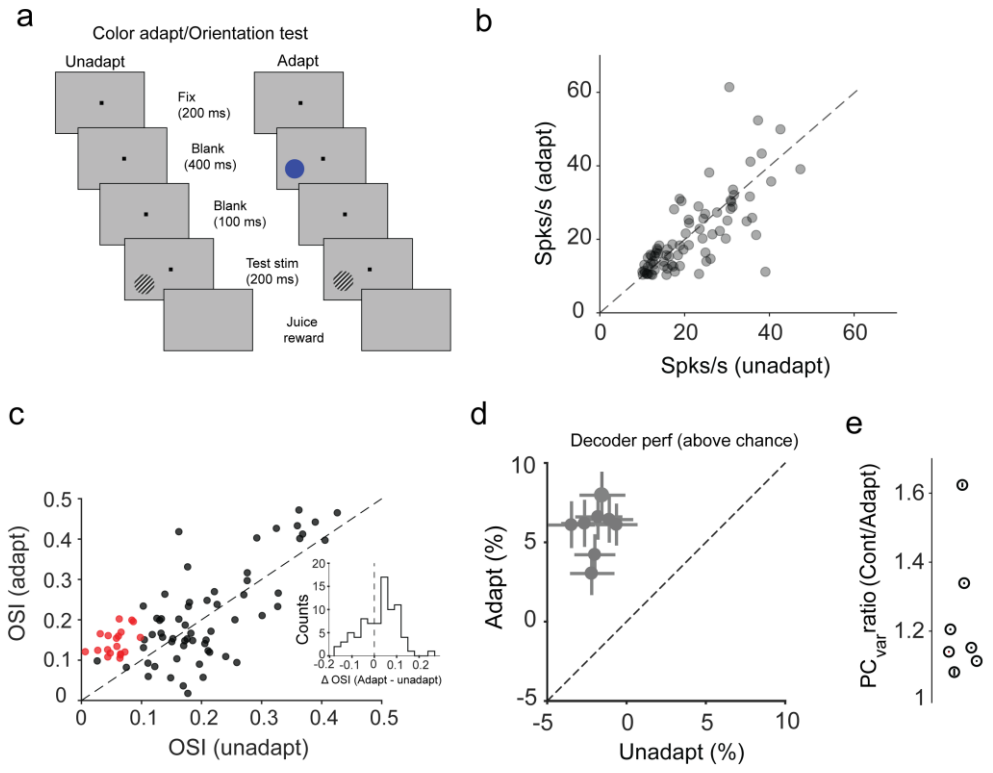

Figure 4. Cross feature color adaptation effects. a Schematic description of experimental design in case of cross feature color adaptation (color adapt/orientation test). **b** Mean peak responses of neurons (n = 80) to oriented stimuli for adapted and unadapted trials. Each gray circle represents a single neuron. **c** Orientation selectivity index (OSI) for neurons in adapted and unadapted conditions. Red circles represent neurons that were untuned to orientation in the unadapted condition but gained significant tuning after color adaptation; black circles represent all other neurons. Inset shows the distribution of change in CSI values (adapt –

unadapt, $\Delta CSI_{mean} = 0.02$) calculated for all neurons. **d** Mean decoder accuracy (%) above chance for classifying neighboring color stimuli based on the response of the neuronal population in each session (gray filled circle, 8 sessions) in unadapted and adapted conditions. Error bars represent s.e.m for the decoder accuracy over multiple iterations of the classifier. **e** Mean value of the ratio of population variance explained by principal components that account for 90% of the variance for each individual session in monkey T. Error bars were evaluated by performing PCA analysis on sub-sampled trials in each condition.

sessions in monkey T). When using this new stimulus set, we found a small but significant decrease in peak responses to color stimuli after orientation adaptation (Fig. 4b; $\Delta FR_{adapt-unadapt} = -3.3 \pm 2.9$ %; $P = 0.02$, Wilcoxon signed-rank test). Similar to our original experiments, cross-feature color adaptation rendered a significant proportion of cells (18%) orientation-tuned despite an initial, pre-adaptation, lack of tuning (Fig. 4c). Furthermore, 28% of the orientation-tuned neurons exhibited a significant sharpening post adaptation ($n = 123$ neurons; $P < 0.05$, Wilcoxon sign rank test, Fig. 4c inset). Cross-feature adaptation yielded an increase in decoder performance to distinguish between pairs of neighboring orientations (separated by 11.25°, Fig. 4d; mean increase: 7.7 ± 0.5%; $n = 8$ sessions). Similar to the previous effects, we observed a significant reduction in the population variance along principal component axis in adapted compared to unadapted conditions (Fig. 4e, Supplementary Fig. 10b). Taken together, these results strengthen our initial findings that cross-feature adaptation during free viewing improves the ability of neuronal populations to distinguish between nearby stimuli lying on an orthogonal feature axis.

Discussion

Natural scenes are characterized by a wide range of features, among which color and orientation represent two major components. While exploring natural scenes, during successive visual fixations, neurons are often exposed to image patches dominated by oriented signals, while subsequent fixations could land on distant image patches where color is the primary feature. It is widely believed that rapid adaptation during natural viewing could play a role in the efficient coding of diverse features (orientation, color, etc.) present in natural scenes[6]. However, this efficient coding hypothesis has emerged from passive fixation experiments in which stimuli varied along a single feature axis. Therefore, whether adaptation to a single feature influences neurons' response to a widely different feature (cross-feature adaptation) such as to influence the accuracy of stimulus encoding has remained unknown.

To our knowledge, our study is the first investigation systematically examining the effects of cross-feature adaptation using a novel free-viewing paradigm whereby animals voluntarily explored stimuli consisting of multiple features (color and orientation) to show that the accuracy of visual cortical populations to discriminate stimuli is improved after cross feature adaptation. In addition, we used more controlled fixation conditions to characterize in greater detail the effect of cross-feature adaptation on neuronal tuning curves and population discrimination performance. Our most surprising finding is that a substantial fraction of visually-responsive neurons that were either untuned or poorly tuned for color or orientation became tuned after adapting to stimuli lying on an orthogonal feature axis, which may lead to a major revision of sensory adaptation and its neural underpinnings. Indeed, untuned neurons are usually ignored in most studies of cortical function, yet we demonstrate that they could play a significant role in the adaptive coding of sensory inputs. Furthermore, the remaining neurons, tuned to color or orientation, significantly improved their tuning after cross-feature adaptation.

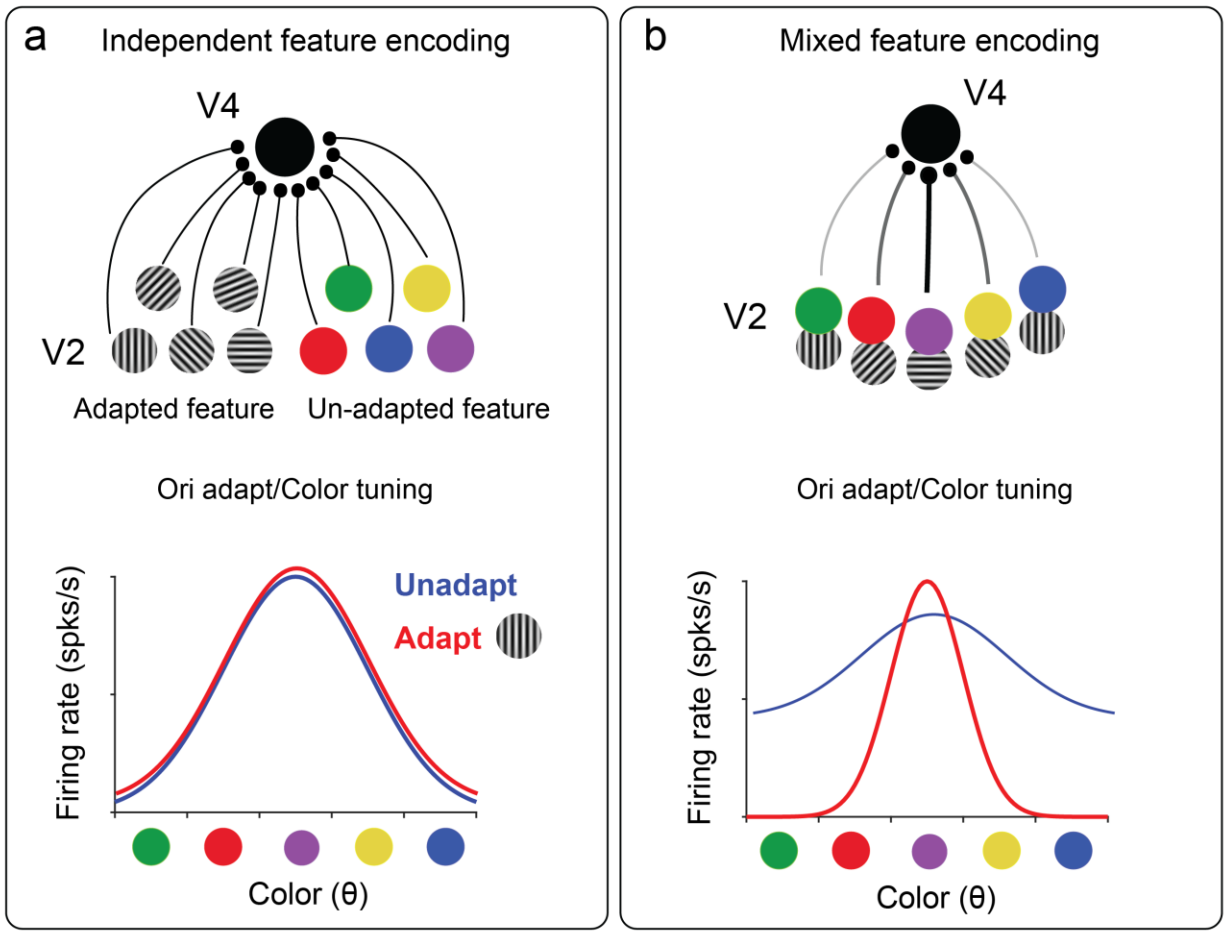

Figure 5. Cross-feature adaptation involves mixed feature selectivity of inputs to area V4. (a) Top: A target V4 neuron (solid black circle) receives heterogeneous orientation and color inputs from upstream neurons (e.g., in area V2) via anatomically non-overlapping/distinct set of channels for each feature (independent feature encoding). This neuron is adapted to a vertical grating (orientation adaptation) and its tuning to color (unadapted feature) is tested. **Bottom:** Schematic representation of tuning curves before (blue) and after adaptation (red) consistent with independent feature encoding, i.e., adaptation to oriented gratings does not affect color tuning. **(b) Top:** In contrast to **a**, a different V4 neuron receives both orientation and color inputs through the same synapses (mixed feature encoding). Some synapses are stronger than others (thick black line compared to faint gray lines) giving rise to broad band tuning for either feature. **Bottom:** Schematic depiction of tuning for this neuron before and after adaptation showing sharpening/emergence of tuning due to adaptation-induced modification of specific synapses (via a reduction of flank responses).

What type of mechanism could possibly explain these adaptive cross-feature effects unreported in previous studies? Our results indicate complex feedforward and intracortical connectivity between cross-feature tuned V4 neurons. While orientation and color modules are believed to lie in separate functional domains, some V4 neurons could receive feedforward and intracortical inputs from a population of cells jointly encoding orientation and color signals[22–24]. Although these inputs may be insufficient to warrant a sharp tuning to cross-feature stimuli, neurons can nonetheless acquire orientation or color selectivity after adaptation provided that the cross-feature inputs are differentially weakened after the brief exposure to the adapting stimulus. This indicates a higher degree of specialization of inputs to neurons in mid-level visual cortical areas than currently assumed.

More specifically, the prevalent feedforward model of feature encoding in V4 predicates that signals corresponding to orthogonal features, such as color and orientation, are transmitted via anatomically separate channels (independent feature encoding model, Fig. 5a, top). However, this model would predict that adaptation to one feature (e.g., orientation) will not alter the strength of inputs carrying information about the other feature (e.g., color). As a result, while orientation tuning of the target neuron is likely to change, the color tuning properties will remain unaffected (Fig. 5a, bottom). Alternately, the inputs to V4 neurons could simultaneously carry a broad range of color and orientation signals (mixed feature encoding model). For instance, Fig. 5b, top, illustrates a V4 neuron receiving mixed weakly tuned color and orientation signals. However, adaptation to a vertically oriented grating will specifically weaken synapses associated with the adapting orientation, which in turn will modify responses to the set of color signals (orthogonal feature) transmitted via the same set of synapses (Fig. 5b, bottom). The emergence of tuning to a specific color/orientation in untuned neurons depends on the heterogeneity of input signals for the adapted feature. For example, if feedforward orientation signals are similar across multiple inputs, adapting to that orientation will lead to a uniform reduction of neuronal responses across all colors instead of a selective decrease. Such an input structure would not lead to the post-adaptation emergence of tuning reported in our study. However, in realistic neural networks, the structure of feedforward inputs to cortical neurons is likely to be diverse, which is probably the main reason why the adaptation effects reported here are heterogeneous, ranging from emergence of tuning to loss of, or unchanged, tuning. Notably, despite this diversity, there was an overall significant increase in orientation and color tuning strength after adaptation and an improvement in stimulus discriminability through the decorrelation of population responses. Thus, specificity of rapid plasticity in neurons coupled with mixed feature selectivity could provide a mechanism for the observed changes in tuning. Our findings indicate a higher degree of specialization in the structure of inputs to mid-level visual cortical neurons beyond that proposed by the independent encoding models reported in previous studies. In fact, neurons with mixed feature selectivity (joint encoding of both color and orientation signals) have been found in macaque V1[23] which could be the source of mixed feature inputs to downstream areas.

Free-viewing a multi-stimulus patch presents a distinct set of challenges as saccades are voluntary (without a fixed trial structure) and the locations of neurons' receptive fields change along with the gaze of the animal. We addressed these challenges by calibrating eye movements and thresholding eye velocity to extract pseudo trials in the unadapted and adapted conditions, and eliminated trials where the receptive fields of neurons covered more than a single stimulus or were close to the stimulus boundaries or the edge of the monitor. While free-viewing allowed us to examine rapid adaptation across features under more naturalistic conditions, we complemented the free-viewing approach with passive fixation experiments for a more detailed characterization of changes in tuning properties. Together, this complementary approach revealed that cross-feature adaptation is a general feature of visual cortical circuits that manifests both in naturalistic and fixed gaze viewing conditions.

A key result in our study is that rapid cross-feature adaptation improves population coding accuracy. We propose that the primary mechanism responsible for this adaptive increase in population coding relies on a reduction in the shared variability among neurons. Indeed, theoretical work has shown that changes in correlated activity in neurons influence stimulus encoding in sensory areas[24–27]. Furthermore, using principal component analysis, recent work[21,22] has shown that learning and decision making are associated with changes in shared variability at the

population level. Employing a similar approach, we found that cross-feature adaptation led to a significant decrease in shared variability along principal component axes that explain most of the response variance (around 90%). This finding was consistent across free-viewing and passive fixation experiments using color and orientation adapters. Our population analysis indicates that rapid cross feature adaptation causes an overall decorrelation in the structure of trial-by-trial population activity. From a functional standpoint, this implies that exposure to an oriented stimulus prepares the color encoding system by decreasing variance across the neural population, thereby enabling a rapid emergence of color tuned responses during successive fixations (hence increasing coding accuracy). Interestingly, rapid adaptation decorrelates neuronal responses to different features (color and orientation) in qualitatively similar ways. Additionally, analysis of iso-feature adaptation data (adapter and test stimuli belonging to the same feature), revealed similar qualitative changes in tuning strength, discriminability and population response variance (Supplementary Figure 11). This indicates that decorrelation could be a general mechanism at the population level to efficiently encode a wide variety of sensory stimuli after adaptation[28]

Surprisingly, there is a complete lack of studies on either rapid or prolonged adaptation in the cross-feature domain with respect to changes in stimulus discriminability. Previous studies have revealed cross-orientation[29] and cross-sensory interactions[30,31], however the role of such interactions on stimulus discriminability has not been explored. Psychophysical evidence of cross-feature adaptation, although of a very different kind than that presented in our study, has been observed in the form of the McCullough effect[32]. Although this color aftereffect due to long-term adaptation (2-4 minutes) implies interaction between features, it is not associated with an improvement (at any time scale) in the discriminability of features, as reported in our study. Furthermore, a more recent study[33] has examined the effects of adaptation (~ 5 s) to contrast and luminosity on the encoding of oriented stimuli to report an improvement in discrimination thresholds post adaptation. However, unlike color/orientation encoding which are believed to be represented by anatomically distinct modules, features such as contrast and luminance are typically represented by the same population of neurons as that encoding for orientation stimuli. Our findings in single neurons and populations are likely to motivate future psychophysics experiments using both synthetic and natural stimuli to directly test the perceptual effects of cross-feature adaptation. Additionally, although we characterized the cross-feature adaptive interactions using well parametrized synthetic stimuli (orientation and color), our work sets the stage for future endeavors to explore rapid adaptation using more complex stimuli found in natural scenes. Adaptive changes in population coding accuracy similar to those shown here may exist in other brain areas. Therefore, examining the adaptive properties of the neural code across the visual system, or other systems, will likely provide important clues about the link between neural population activity and perception during naturalistic viewing.

Methods

All experiments were performed in accordance with protocols approved by the U.S. National Institutes of Health Guidelines for the Care and Use for Experimental Procedures and the Institutional Animal Care and Use Committee (IACUC) at the University of Texas Health Science Center at Houston. Data presented in this study was collected from three adult male rhesus monkeys (*Macaca mulatta;* T: 14 years old, 13 kg; M: 10 years old, 10 kg and R: 7 years old, 12 kg). A titanium head post was surgically implanted in the medial frontal region with the help of

multiple anchor screws. After a recovery period of 4 weeks, both animals were trained for a month on visual fixation tasks (to be used later for the recordings) involving at least 1000 trials per session. After the monkeys learned to complete multiple sessions in a single day, we implanted a 96-channel Utah array in monkey T and R and a 64-channel Utah array in monkey M in area V4 (left hemisphere in all animals). Coordinates for craniotomies were estimated based on locating the superior temporal sulcus (STS) and the lunate sulcus by comparing MRI images from the animals to brain atlases. During surgery, the grooves corresponding to the STS and the lunate sulcus were used to guide the implantation of the array. Arrays were roughly implanted at the crown of the pre-lunate gyrus. Post-surgery, animals went through a 2-3 week recovery period and additional training for re-acclimatization with previously learned fixation tasks before we started recording.

Visual stimuli for single unit recordings. Visual stimuli were presented on a gamma corrected CRT monitor (HP p1230). To measure color tuning we used a set of 16 equiluminant colors (9.35 ± 0.01 cd/m^2) spanning the full color gamut of the monitor and presented at the maximum saturation allowed by the monitor[20]. These 16 colors were uniformly spaced (in steps of 22.5º) when plotted in the CIELUV color space[34,35] (Fig. 2a) which is designed to be perceptually uniform. L represents the luminosity, and u, v represent the chromaticity coordinates in a two dimensional perceptually uniform color space. Luv coordinates were measured for each color and the gray background using a Tektronix photometer (J17 Lumacolor) before the start of each recording session. These colors were presented on a neutral gray background designed to have the same luminosity as the color stimuli (see Extended Data Table 1). Grating stimuli consisted of 16 orientations spanning 0° to 180° in steps of 11.25°. The mean luminosity of the gratings was matched to that of the color patches and the gray background. Visual stimuli were presented binocularly; eye tracking was performed for only one of the eyes.

Behavioral task. Two monkeys were trained to fixate on a small point (0.2 deg) within a small rectangular 1-deg window at the center of a cathode ray tube (CRT) monitor while remaining head fixed. If at any point during the trial, eye position exceeded 0.25 deg outside the boundaries of the rectangular box, then the trial was automatically aborted. Animals were rewarded with juice at the end of each trial in which fixation was successfully maintained for the entire duration of stimulus presentation. Eye movements were monitored throughout the recording session using an infrared eye tracking system (EyeLink II, SR Research) at a 1-kHz sampling rate. Stimulus presentation was recorded and synchronized with the neural data using a programmable Experiment Control Module device (FHC Inc.).

Electrophysiological recordings. We recorded extracellular activity as action potentials and local field potentials simultaneously from all 96 channels (monkey T, R) and 64 channels (monkey M) of three chronically implanted Utah arrays (Blackrock Microsystems) while animals performed passive fixation tasks. The interelectrode spacing in these arrays was 400 µm. Data was recorded at a sampling rate of 30 kHz using a Cerebus Neural Signal Processor (Blackrock Microsystems, LLC). Spike waveforms above threshold (~ 4 sd above the amplitude of the noise signal) were saved and sorted post data acquisition using Plexon's Offline Sorter. Spike waveforms were manually sorted with Plexon's offline sorter program using waveform clustering parameters such as spike amplitude, spike width, timing of the valley and peak. Units that formed well separated clusters in principal component space were identified as single or multi units. Units that had more than 2% of their post sorted spikes within the refractory period (2ms) were classified as multi units

and were eliminated from the analysis[36]. The remaining single units were subsequently analyzed using custom scripts in MATLAB. We treated each recording session performed on a particular day as an independent session, which is a common approach in multiple labs[20,21,37–39] as it is difficult to determine whether the same units were recorded on subsequent days over the course of several months.

RF mapping. To map the RFs of the single units we divided the right visual field into a 3 x 3 grid consisting of 9 squares with each square covering 8 x 8 degrees of visual space. The entire grid covered 24 x 24 degrees of visual space. Each of the 9 squares was further subdivided into a 6 x 6 grid. In each trial 1 out of the 9 squares was randomly chosen and RF mapping stimuli was presented at each of the 36 locations in a random order. The RF mapping stimuli consisted of a reverse correlation movie with red, blue, green and white patches (~1.33 degrees each). A complete RF session comprised of 10 presentations of the RF mapping stimuli in each of the 9 squares forming the 3 x 3 grid. We averaged the responses over multiple presentations to generate the RF heat maps. RF mapping was done at the beginning of each recording session as it was impossible to track the same neurons over the course of the recordings which lasted several months. The position and size of the target stimulus for examining tuning was chosen each day so that it roughly covered the overlapping RFs of only a subset of neurons. Neurons whose RFs could not be covered completely by the chosen target were not included in the analysis. This ensured that the size of the target could be kept small so as to minimize surround stimulation.

Free-viewing adaptation task. A four-panel static stimuli (Fig. 1e) was designed to evaluate cross-feature adaptation in a free-viewing paradigm. The upper right quadrant was a grey isoluminant control, the upper left quadrant was the adapter stimulus, and the lower quadrants were test stimuli. To assess responses to color after adaptation to an oriented grating, we used a grating adapter stimulus oriented at 135° with a spatial frequency of ~2.8 cycles/deg. Grating parameters were chosen to elicit responses from as many neurons recorded by the array. The hue angle corresponding to the 2 test stimuli were 45 and 67.5° (neighboring stimuli) and were placed in the lower left and right quadrants respectively. To assess response to oriented gratings following adaptation to color, we used a color adapter stimulus of 0 degrees of hue angle. The oriented gratings were 112.5 and 135° for the bottom left and right quadrants respectively. Before presenting the static task stimulus, eye position was first calibrated with respect to the monitor. The task stimulus was presented on the monitor for a total duration of roughly 1 hr in each session. A drop of juice was automatically given to the animal at regular intervals provided its point of gaze was on the stimulus monitor. Saccades and fixations were analyzed offline, and separated by a velocity threshold of 100 deg/s[40]. We extracted 'pseudo-trials' from the free-viewing recordings based on the sequence and location of fixations with respect to the task stimulus. Unadapted trials were defined as those in which the animal first fixated on the isoluminant grey quadrant (upper right), and then fixated on one of the two lower test stimulus quadrants. Adapted trials were defined as those when the animal first fixated on the adapter quadrant (upper left) and then fixated on one of the two lower stimulus quadrants. Fixation-related variables such as duration of fixations on test or adapter stimuli, velocity and direction of microsaccades, pupil size during fixations were analyzed to show that these variables are not significantly different in the adapted and unadapted trials. Additionally, only fixations for which the full RFs of neurons were confined to one quadrant and did not include the edge of the monitor boundaries or the boundaries separating the different stimuli were included in the analysis (Supplementary Fig. 4).

Sobel filter analysis. We computed the orientation content of images by applying a Sobel filter[41–43] to each image. For each pixel we determined both the orientation and the orientation magnitude by calculating the partial derivative of brightness in a 3x3 kernel. The orientation was obtained by calculating the arc tangent of the vertical component divided by the horizontal one. The orientation magnitude of the local gradient was calculated from the square root of the sums of the squares of the partial derivatives of the brightness in the vertical and horizontal directions. We then determined the orientation magnitude histogram of an image patch as the number of pixels at each particular orientation (collapsed to a 0º-180º in 5º bins) weighted by the magnitude of the gradient at that pixel. We subsequently calculated the mean orientation and orientation selectivity index (OSI; Fig. 1b) of image patches by extracting the Fourier components from the orientation magnitude histogram for each patch. The Sobel filter analysis was performed on sub-patches of the natural images in a 50 x 50 pixel window that was moved horizontally and vertically by 10 pixels to cover the entire image.

Statistical model of visual exploration of natural scenes. We generated a distribution of saccade amplitude and direction (Supplementary Fig. 2) from the free-viewing experiments described above. Based on these statistics, we generated pseudo-saccades from randomly chosen starting points on a natural image battery (n = 940) from the McGill calibrated color image data base (McGill Vision research) to simulate unrestrained visual exploration. We analyzed a total of 282,000 saccades across all images (300 saccades per image). The size of image patches was chosen based on mean receptive field size of our V4 neurons. For every pseudo-saccade connecting two patches of a natural image, we quantified the strength of orientation and color signals. Orientation signals were calculated by computing an orientation selectivity index (OSI) using a Sobel filter (see Methods). Color signals were quantified by analyzing the distributions of the red, green and blue channel values across all pixels within a patch (values lying between 0 to 255). A patch was considered to be 'colored' if it met the following requirements: a) each of the peaks of the R, G and B channel distributions were not located within a threshold Δ (set at 30) to either 0 or 255 (black or white patches). b) The difference in the peak locations for each channel were not closer than ±Δ (to rule out gray patches). c) The patch did not have significant orientation signals based on the Sobel filter analysis. Patches were considered 'oriented' if there was significant tuning (Rayleigh's test, pval <0.05) based on Sobel filter analysis and did not have color information based on the criteria presented above. To ensure that patches with no significant orientation tuning did not simply contain multiple orientations (multiple peaks in their OSI distribution), we eliminated from the analysis those patches containing more than one peak in their OSI distribution, where peaks were defined as local maxima in the OSI distribution > 3 s.d. above the mean. For each image we analyzed 300 saccades to calculate how often saccades connected two patches with dissimilar/similar features.

Color and orientation tuning. To determine the color/orientation tuning of V4 neurons we calculated the tuning curve from multiple presentations (N ~ 30/per stimuli) of the chosen stimulus feature (color patches/gratings). For each such tuning curve, we calculated the color/orientation selectivity index (CSI/OSI) in the following way: $CSI = \frac{|\sum r_i e^{\theta_i}|}{\sum_i r_i}$ where r_i is the response to a particular color/orientation with angular position θ_i on the color/orientation space. Responses r_i were vectorially summed and then normalized by the sum of the responses for all colors. To control for the effect of noise on estimation of tuning curves, neurons with peak firing rates < 10 spks/s were removed from the analysis. CSI lies between 0 and 1, where a value of 0 represents no tuning

and a value of 1 indicates that the neuron is highly tuned for a specific color. To evaluate whether the neuron's tuning was statistically significant, we used the Rayleigh test for non-uniformity in circular data[9,20,44]. Rayleigh's test is a statistical test used to determine whether a circular distribution (which in our case is the circular tuning curve with firing rates) has a preferred direction, i.e., a preferred color the neuron is tuned to ($P < 0.05$). The null hypothesis is that the circular tuning curve represents a uniform circular distribution and no preferred direction exists ($P > 0.05$). We evaluated CSI and the p-values of the tuning curves in sliding windows (size 200ms, sliding by 5 ms) from the stimulus responses measured separately for unadapted and adapted trials. We performed Holm-Bonferroni correction for multiple comparisons on the p-values. To evaluate the preferred color/orientation (PC/PO) we selected the tuning curve with the highest CSI/OSI which passed the Rayleigh test for non-uniformity ($P < 0.05$). This tuning curve was then used to calculate PC/PO in the following way: $PC = tan^{-1}\left(\frac{Im(\sum r_i e^{\theta_i})}{Re(\sum r_i e^{\theta_i})}\right)$ where Im and Re stands for the imaginary and real parts of the complex sum. We evaluated tuning latency (Fig. 3f) as the first time point where the neuron exhibited significant tuning to a feature ($p < 0.05$, Rayleigh test). To eliminate the effect of noise in evaluating tuning strength and preferred stimulus we eliminated neurons with peak firing rates < 5Hz. Circular statistics was computed using the CircStat Toolbox [45] for MATLAB.

Adaptation task (passive fixation). In adaptation trials an adapter of a particular feature (color or orientation) preceded the presentation of a tuning test stimulus of another feature. The adapter was presented for 400 ms and after a 50 ms delay (gray screen), a randomly chosen tuning stimulus was presented briefly for 200 ms. In unadapted trials the presentation of the tuning stimuli was not proceeded by an adapter. A complete session involved randomly interleaved adapted and unadapted trials (no adapter). The adapting stimulus was chosen so that it activated a majority of the recorded neurons in a session. We recorded close to 1000 trials in these sessions split roughly equally between unadapted and adapted conditions. The duration between the last frame of the tuning stimulus and the first frame of the adapting stimulus in the next trial was at least 4.6 s which allowed sufficient time for the responses to return to baseline.

Noise correlation analysis: Spike count correlations between pairs of neurons was evaluated using the Pearson's correlation coefficient defined as follows:

$$r_{sc} = \frac{\sum_{k=1}^{N}(r_{ik} - r_j)(r_{jk} - r_j)}{N\sigma_i\sigma_j} = \frac{\sum_{k=1}^{N} r_{ik}r_{jk} - r_i r_j}{N\sigma_i\sigma_j}$$

Where N is the number of trials, r_{ik} is the firing rate of neuron i in trial k, r_i is the mean firing rate (averaged over trials) evaluated in a 200 ms window aligned with test stimulus onset and matching the duration of test stimuli presentation, and σ_i is the standard deviation of the responses of the neuron i. Neurons with peak firing rates < 5 spks/s were not included in the noise correlation analysis. Additionally, trials in which the absolute values of the z-scored firing rates of either neuron exceeded three times the mean were eliminated from the analysis. Finally, we averaged the noise correlation across all stimuli for a particular feature to report mean correlated activity in neuronal pairs. Noise correlations were calculated for all pairs both before and after adaptation. In case of the free-viewing recordings, spike counts were evaluated for the duration of each fixation on the test stimuli.

Principal component analysis of population activity: We performed principal component analysis (PCA) on a trial-by-trial basis for the entire population of neurons[21,22], in both unadapted and adapted conditions for each experimental paradigm. Principal Component analysis was performed on responses in each trial (e.g., firing rates during fixations) of all recorded neurons in the unadapted condition, i.e., PCA was performed on a M x N matrix where M denotes trials and N the number of neurons. To control for the effect of high variance in single neuron responses (outliers) dominating the PCA, we removed neurons whose variance exceeded 2 std above the mean variance of all the neurons in a session. We then projected the trial-by-trial activity of the same neurons during the adaptation condition onto the PC axis obtained for the control condition and examined the ratio of the variance explained by each principal component in the control and adaptation condition by focusing on the mean ratio for those PCs that captured 90% of the variance of the population response in the control condition. To obtain error estimates for ratio values, PCA analysis was repeated 100 times with a different set of sub-sampled trials (same number) in unadapted and adapted conditions.

Decoder analysis. We used linear discriminant analysis[46–48] to examine whether cross-feature adaptation enhanced the ability of neural populations to discriminate between nearby stimuli. We analyzed decoder accuracy for pairs of nearest neighbor stimuli in feature space, i.e., separated by 11.25° in the case of gratings and 22.5° in the case of color stimuli. The decoder was trained on spike counts evaluated in 200 ms (0-200 ms post tuning stimulus onset) for a subset of the trials. In the case of free-viewing recordings, spike counts calculated for the fixation window were used as inputs to the decoder. The classifier was trained on 70% of the trials and performance was tested on the remaining 30%. We repeated this classification process 500 times with different training and testing sets drawn randomly from the trials from a session. Decoder performance was averaged over the number of iterations and evaluated for both unadapted and adapted conditions. We subtracted chance values of decoder performance for a pair of stimuli (50%) from the actual values and thus reported decoder accuracy values above chance for both free-viewing and passive fixation experiments.

Statistical analysis. Quantification and statistical test for tuning was performed using the Rayleigh test implemented with the CircStat Toolbox[45]. Correlations were quantified using either Pearson's correlation or Spearman's rank correlation to account for linear/non-linear trends as applicable. We used the non-parametric Wilcoxon's signed rank test (two tailed) to quantify whether distributions had medians significantly greater than or less than zero. In case of two distributions with unequal sample size we used the Wilcoxon rank sum test to examine the statistical significance of the difference in their medians.

References

1. Simoncelli, E. P. & Olshausen, B. A. Natural image statistics and neural representation. *Annu. Rev. Neurosci.* **24**, 1193–1216 (2001).

2. Olshausen, B. A. & Field, D. J. Natural image statistics and efficient coding. *Netw. Comput. neural Syst.* **7**, 333–339 (1996).

3. Field, D. J. Relations between the statistics of natural images and the response properties

of cortical cells. *Josa a* **4**, 2379–2394 (1987).

4. Weber, A. I., Krishnamurthy, K. & Fairhall, A. L. Coding principles in adaptation. *Annu. Rev. Vis. Sci.* **5**, 427–449 (2019).

5. Yarbus, A. L. Eye Movements During Perception of Complex Objects. in *Eye Movements and Vision* (1967). doi:10.1007/978-1-4899-5379-7_8.

6. Dragoi, V., Sharma, J., Miller, E. K. & Sur, M. Dynamics of neuronal sensitivity in visual cortex and local feature discrimination. *Nat. Neurosci.* (2002) doi:10.1038/nn900.

7. Tolhurst, D. J., Tadmor, Y. & Chao, T. Amplitude spectra of natural images. *Ophthalmic Physiol. Opt.* **12**, 229–232 (1992).

8. Reinagel, P. & Zador, A. M. Natural scene statistics at the centre of gaze. *Netw. Comput. Neural Syst.* **10**, 341 (1999).

9. Conway, B. R., Moeller, S. & Tsao, D. Y. Specialized color modules in macaque extrastriate cortex. *Neuron* **56**, 560–573 (2007).

10. Tanigawa, H., Lu, H. D. & Roe, A. W. Functional organization for color and orientation in macaque V4. *Nat. Neurosci.* **13**, 1542 (2010).

11. Dragoi, V., Rivadulla, C. & Sur, M. Foci of orientation plasticity in visual cortex. *Nature* **411**, 80–86 (2001).

12. Müller, J. R., Metha, A. B., Krauskopf, J. & Lennie, P. Rapid adaptation in visual cortex to the structure of images. *Science.* **285**, 1405–1408 (1999).

13. Gutnisky, D. A. & Dragoi, V. Adaptive coding of visual information in neural populations. *Nature* **452**, 220 (2008).

14. Dragoi, V., Sharma, J. & Sur, M. Adaptation-induced plasticity of orientation tuning in adult visual cortex. *Neuron* **28**, 287–298 (2000).

15. Patterson, C. A., Wissig, S. C. & Kohn, A. Distinct effects of brief and prolonged adaptation on orientation tuning in primary visual cortex. *J. Neurosci.* **33**, 532–543 (2013).

16. Sclar, G., Lennie, P. & DePriest, D. D. Contrast adaptation in striate cortex of macaque. *Vision Res.* **29**, 747–755 (1989).

17. Solomon, S. G., Peirce, J. W., Dhruv, N. T. & Lennie, P. Profound contrast adaptation early in the visual pathway. *Neuron* **42**, 155–162 (2004).

18. Kohn, A. & Movshon, J. A. Neuronal adaptation to visual motion in area MT of the macaque. *Neuron* **39**, 681–691 (2003).

19. Kohn, A. & Movshon, J. A. Adaptation changes the direction tuning of macaque MT neurons. *Nat. Neurosci.* **7**, 764–772 (2004).

20. Nigam, S., Pojoga, S. & Dragoi, V. A distinct population of heterogeneously color-tuned neurons in macaque visual cortex. *Sci. Adv.* **7**, eabc5837 (2021).

21. Ni, A. M., Ruff, D. A., Alberts, J. J., Symmonds, J. & Cohen, M. R. Learning and attention reveal a general relationship between population activity and behavior. *Science.* **359**, 463–465 (2018).

22. Valente, M. *et al.* Correlations enhance the behavioral readout of neural population activity in association cortex. *Nat. Neurosci.* **24**, 975–986 (2021).

23. Garg, A. K., Li, P., Rashid, M. S. & Callaway, E. M. Color and orientation are jointly coded and spatially organized in primate primary visual cortex. *Science.* **364**, 1275–1279 (2019).

24. Ehud, Z., Michael, N., S. & William, T., N. Correlated neuronal discharge rate and its implications for psychophysical performance. *Nature* **370**, 140–143 (1994).

25. Abbott, L. F. & Dayan, P. The effect of correlated variability on the accuracy of a population code. *Neural Comput.* **11**, 91–101 (1999).

26. Averbeck, B. B., Latham, P. E. & Pouget, A. Neural correlations, population coding and computation. *Nat. Rev. Neurosci.* **7**, 358–366 (2006).

27. Shadlen, M. N. & Newsome, W. T. The variable discharge of cortical neurons: implications for connectivity, computation, and information coding. *J. Neurosci.* **18**, 3870–3896 (1998).

28. Ni, A. M., Huang, C., Doiron, B. & Cohen, M. R. A general decoding strategy explains the relationship between behavior and correlated variability. *Elife* **11**, e67258 (2022).

29. Hu, J. M., Qian, M. Z., Tanigawa, H., Song, X. M. & Roe, A. W. Focal electrical stimulation of cortical functional networks. *Cereb. Cortex* **30**, 5532–5543 (2020).

30. Mehta, A. D., Ulbert, I. & Schroeder, C. E. Intermodal selective attention in monkeys. I: distribution and timing of effects across visual areas. *Cereb. cortex* **10**, 343–358 (2000).

31. Ibrahim, L. A. *et al.* Cross-modality sharpening of visual cortical processing through layer-1-mediated inhibition and disinhibition. *Neuron* **89**, 1031–1045 (2016).

32. McCollough, C. Color adaptation of edge-detectors in the human visual system. *Science.* **149**, 1115–1116 (1965).

33. Ghodrati, M., Zavitz, E., Rosa, M. G. P. & Price, N. S. C. Contrast and luminance adaptation alter neuronal coding and perception of stimulus orientation. *Nat. Commun.* **10**, 1–13 (2019).

34. Bohon, K. S., Hermann, K. L., Hansen, T. & Conway, B. R. Representation of perceptual color space in macaque posterior inferior temporal cortex (the V4 complex). *Eneuro* **3**, (2016).

35. CIE, C. I. E. 15: 2004 COLORIMETRY. *Comm. Int. l'Eclairage,* (2004).

36. Conway, B. R. & Livingstone, M. S. Spatial and temporal properties of cone signals in alert macaque primary visual cortex. *J. Neurosci.* **26**, 10826–10846 (2006).

37. Ruff, D. A. & Cohen, M. R. Attention can either increase or decrease spike count

correlations in visual cortex. *Nat. Neurosci.* **17**, 1591 (2014).

38. Milton, R., Shahidi, N. & Dragoi, V. Dynamic states of population activity in prefrontal cortical networks of freely-moving macaque. *Nat. Commun.* **11**, 1–10 (2020).

39. Smith, M. A. & Kohn, A. Spatial and Temporal Scales of Neuronal Correlation in Primary Visual Cortex. *J. Neurosci.* **28**, 12591–12603 (2008).

40. Smeets, J. B. J. & Hooge, I. T. C. Nature of variability in saccades. *J. Neurophysiol.* **90**, 12–20 (2003).

41. Coppola, D. M., Purves, H. R., McCoy, A. N. & Purves, D. The distribution of oriented contours in the real world. *Proc. Natl. Acad. Sci.* **95**, 4002–4006 (1998).

42. Dragoi, V., Turcu, C. M. & Sur, M. Stability of cortical responses and the statistics of natural scenes. *Neuron* **32**, 1181–1192 (2001).

43. Dragoi, V. & Sur, M. Image structure at the center of gaze during free viewing. *J. Cogn. Neurosci.* **18**, 737–748 (2006).

44. Sanada, T. M., Namima, T. & Komatsu, H. Comparison of the color selectivity of macaque V4 neurons in different color spaces. *J. Neurophysiol.* **116**, 2163–2172 (2016).

45. Berens, P. CircStat: a MATLAB toolbox for circular statistics. *J Stat Softw* **31**, 1–21 (2009).

46. Averbeck, B. B., Crowe, D. A., Chafee, M. V. & Georgopoulos, A. P. Neural activity in prefrontal cortex during copying geometrical shapes. II. Decoding shape segments from neural ensembles. *Exp. Brain Res.* **150**, 142–153 (2003).

47. Pesaran, B., Pezaris, J. S., Sahani, M., Mitra, P. P. & Andersen, R. A. Temporal structure in neuronal activity during working memory in macaque parietal cortex. *Nat. Neurosci.* **5**, 805 (2002).

48. Nigam, S., Pojoga, S. & Dragoi, V. Synergistic Coding of Visual Information in Columnar Networks. *Neuron* **104**, (2019).

Supplementary Information

Adaptive coding across visual features during free-viewing and fixation conditions

Sunny Nigam, Russell Milton, Sorin Pojoga, Valentin Dragoi

R	G	B	u	v	L (cd/m^2)
173	0	1	0.273	0.548	9.32
143	71	0	0.204	0.556	9.29
117	86	0	0.155	0.551	9.36
81	99	0	0.109	0.566	9.46
0	104	67	0.093	0.516	9.33
0	100	83	0.105	0.473	9.30
0	97	88	0.107	0.455	9.43
0	96	91	0.108	0.446	9.30
0	96	96	0.112	0.434	9.47
0	95	101	0.115	0.420	9.48
0	95	117	0.126	0.382	9.33
118	0	181	0.189	0.236	9.36
152	0	129	0.219	0.341	9.30
159	0	100	0.230	0.393	9.32
164	0	94	0.241	0.430	9.34
168	0	71	0.255	0.483	9.33
Neutral gray stimulus					
88	88	88	0.137	0.451	9.35

Supplementary Table 1. Color stimulus properties. Luv coordinates and luminance values for color stimuli and neutral gray screen. Mean luminance 9.35 ± 0.01 cd/m^2.

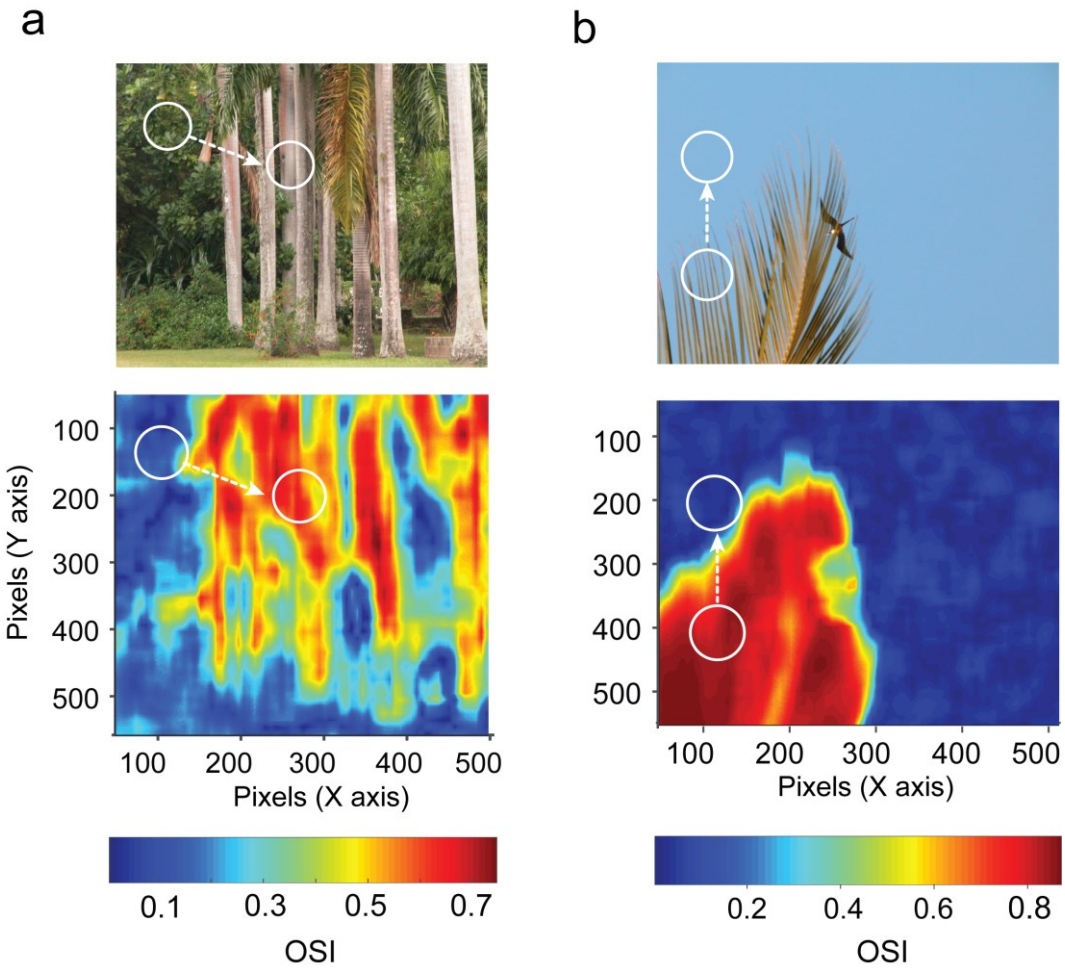

Supplementary Fig. 1 Local orientation analysis of natural scenes. (a) Natural scene (top) and pixel by pixel characterization of mean orientation quantified by Orientation Selectivity Index (OSI) using a Sobel filter. **(b)** Same as in **a** except for a different example natural scene. White circles represent schematic description of position of receptive fields and how feature properties change due to eye movements (dotted white arrow) from one fixation to the other.

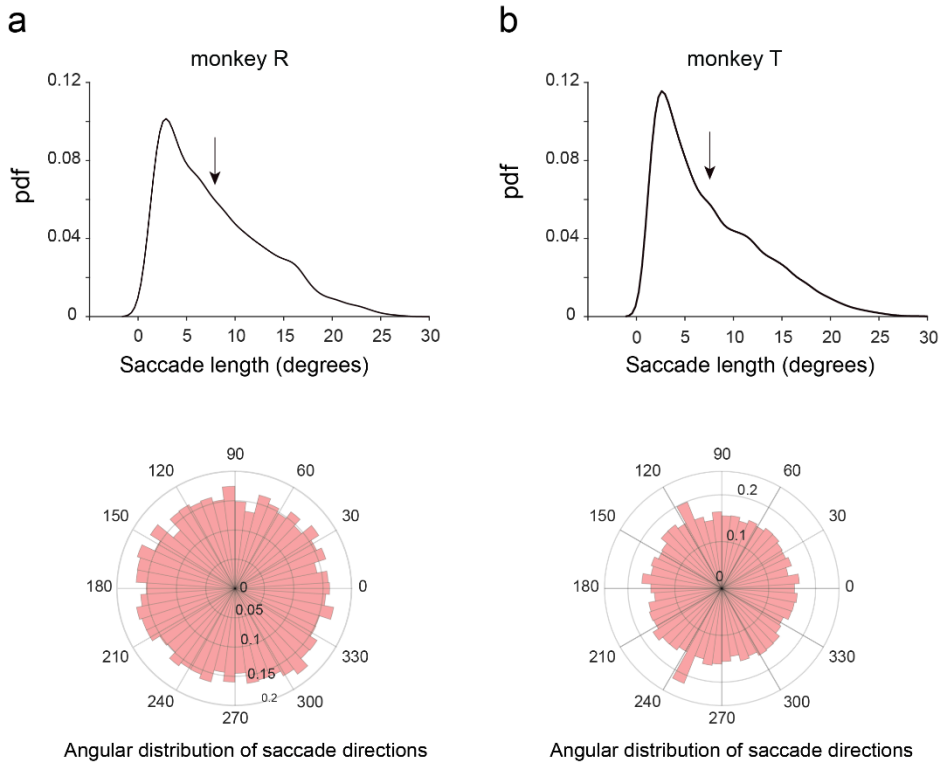

Supplementary Fig. 2 Distribution of saccade length and direction during free-viewing. (a) Top: Probability density function of saccade lengths (n = 11253, mean = 7.9 ± 0.05 deg) made by monkey R, pooled across all sessions during free-viewing of stimuli described in Fig. 1e. Bottom: Distribution of the direction of saccades (circular mean = 1.2°) for the same animal. (b) Top and bottom represent the saccade length and direction distributions for monkey T (n = 25250, mean saccade length = 7.6 ± 0.03 deg and circular mean = -2.8°).

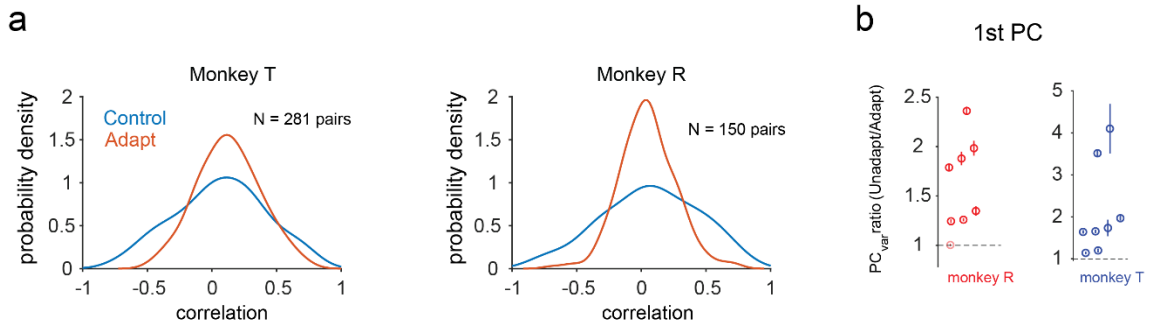

Supplementary Fig. 3 Cross feature adaptation modifies the structure of pairwise and population correlations in free-viewing experiments. (a) Probability density function of mean noise correlations (N = 281 pairs, monkey T; N = 150 pairs, monkey R) averaged over test stimuli in adapted (orange) and unadapted (blue) conditions. ($\langle r_{sc}^{ad} \rangle$ = 0.08±0.01; $\langle r_{sc}^{unad} \rangle$ = 0.09±0.01; Wilcoxon signed rank test, P > 0.05; σ^2_{adapt} =0.053, $\sigma^2_{unadapt}$ =0.024; two-sample F-test, P < 0.0001). **(b)** Ratio of the variance in trial-by-trial population activity explained by the 1st principal component in unadapted and adapted conditions for monkey R (red open circles) and monkey T (blue open circles). Each open circle represents the ratio evaluated for an individual session. Error bars were evaluated by performing PCA analysis on sub-sampled trials in each condition. Light shaded circles represent sessions where the ratio was not significantly greater than 1.

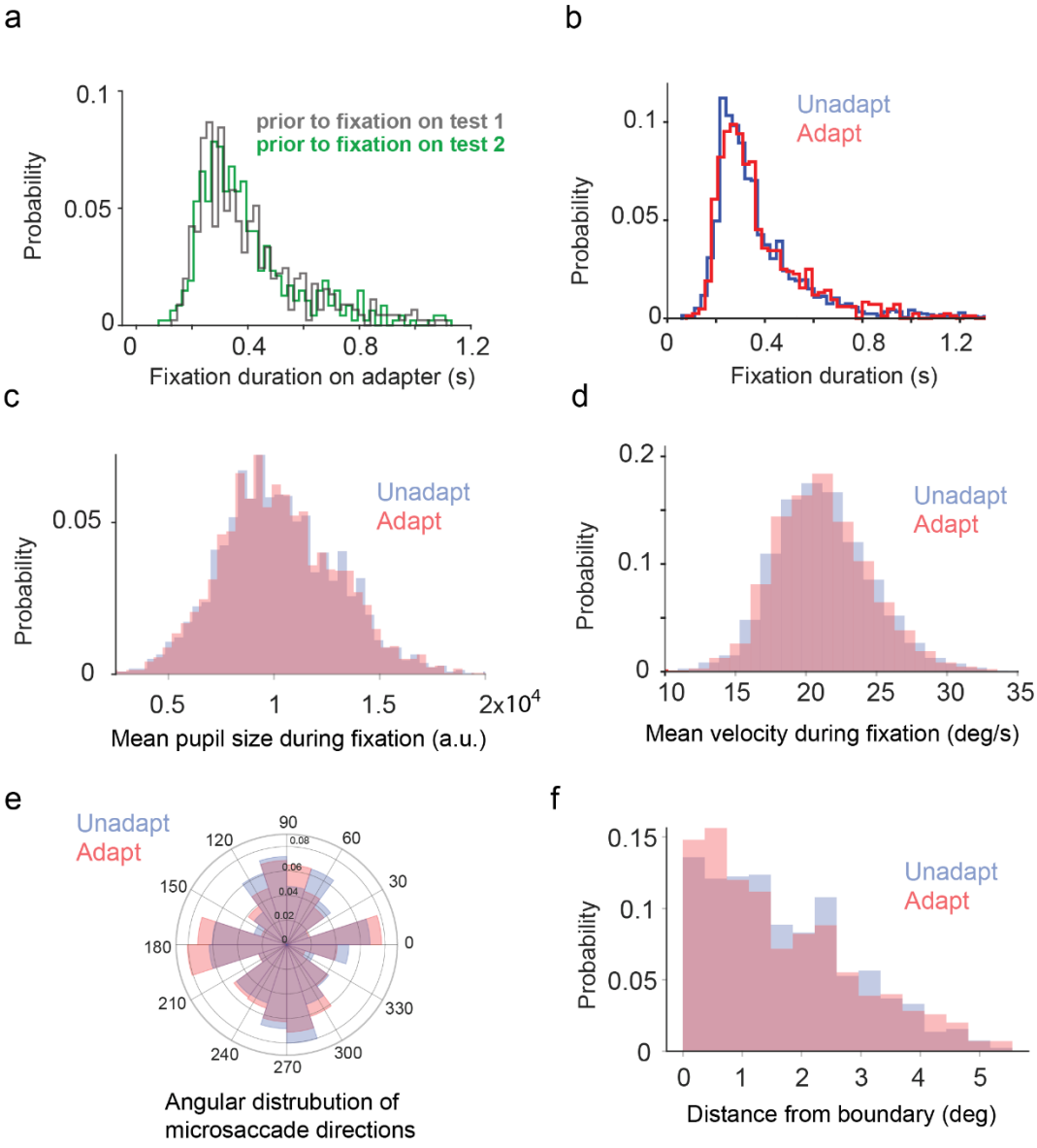

Supplementary Fig. 4 Fixation properties are not significantly different across conditions during free-viewing. (a) Distribution of fixation durations on the adapter prior to fixation on test stimuli 1 (gray histogram) and 2 (green histogram) ($P > 0.05$, Wilcoxon rank sum test). **(b)** Distribution of fixation durations (FD) on test stimuli for unadapted and adapted trials (FD_{unad} = 380 ± 5 ms; FD_{ad} = 385 ± 7 ms; $P > 0.05$, Wilcoxon rank sum test). **(c)** Distribution of mean pupil size (PS) during fixations on test stimuli for unadapted and adapted trials (PS_{unad} = 1.03e4 ± 64 a.u; PS_{ad} = 1.04e4 ± 126 a.u.; $P > 0.05$, Wilcoxon rank sum test). **(d)** Distribution of mean velocity (v) during fixations on test stimuli for unadapted and adapted trials (v_{unad} = 21.3 ± 0.1 deg/s ms; v_{ad} = 21.5 ± 0.2 deg/s; $P > 0.05$, Wilcoxon rank sum test). **(e)** Distribution of microsaccade directions detected during fixations on test stimuli in unadapted and adapted conditions **(f)** Distribution of mean distance (d) of edges of neurons receptive fields from stimulus boundaries during adapted and unadapted trials. (d_{unad} = 1.69 ± 0.02 deg; d_{ad} = 1.66 ± 0.04 deg; $P > 0.05$, Wilcoxon rank sum test).

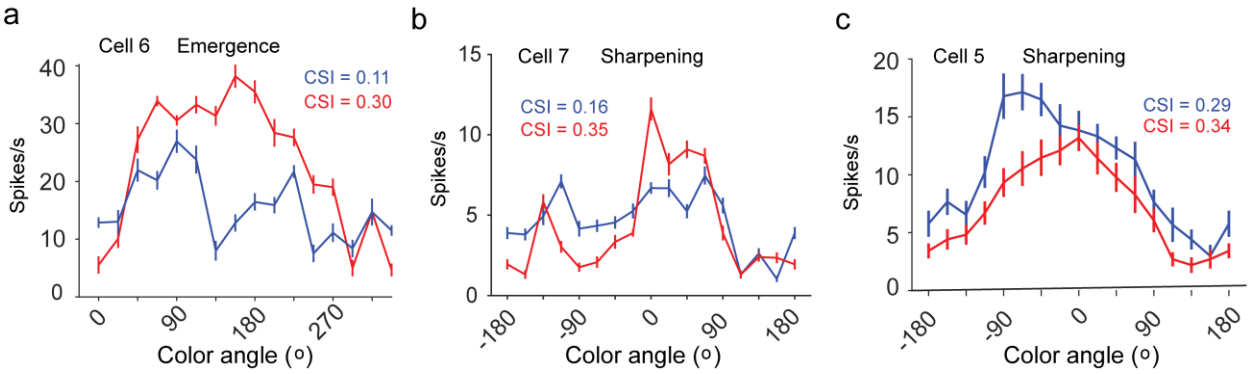

Supplementary Fig. 5 Emergence and sharpening of color tuning after adaptation to oriented gratings. (a) Example cell untuned to color in unadapted condition (blue) showing emergence of tuning to color after being adapted to a grating (red). **(b, c)** Two example cells exhibiting sharpening of existing tuning post adaptation. Solid lines mean responses to color stimuli and errorbars represent s.e.m. Red curves represent adapted condition whereas blue curves represent tuning in unadapted condition.

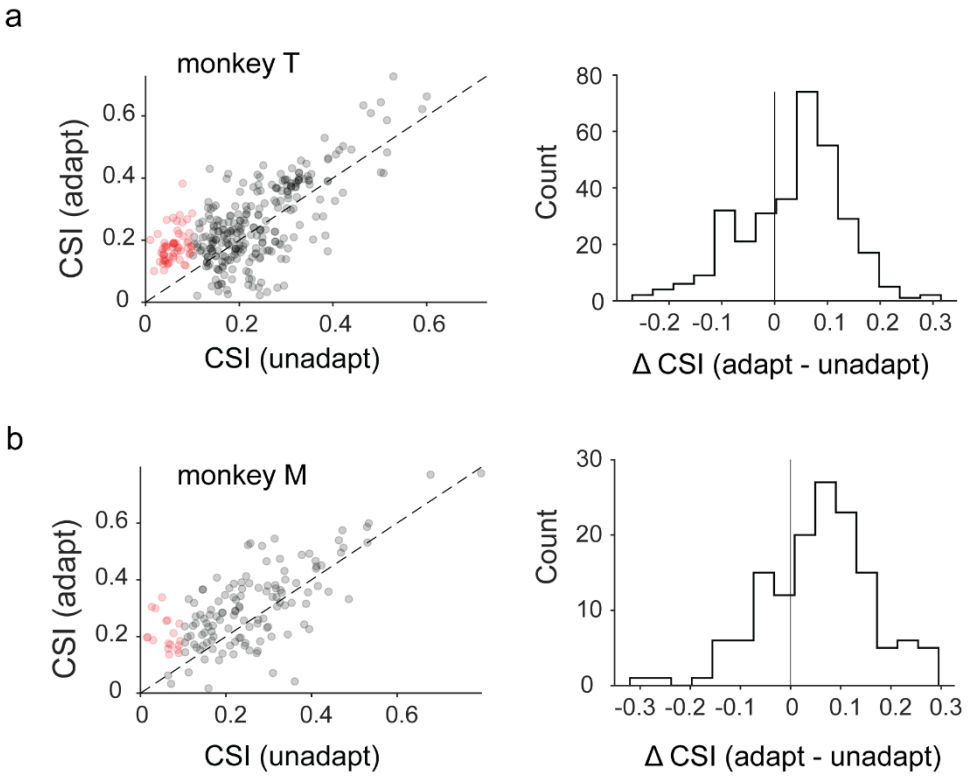

Supplementary Fig. 6 Cross feature adaptation sharpens color tuning in neural populations. **(a)** Left: Color selectivity index (CSI) for neurons in adapted and unadapted conditions (Monkey T, 263 neurons). Red circles represent neurons that were untuned to color in the unadapted condition but gained significant color tuning after orientation adaptation. Black circles represent all other neurons. **Right:** distribution of change in CSI values (adapt – unadapt, $\Delta CSI_{mean} = 0.04 \pm 0.003$, Wilcoxon signed rank test, $P < 0.0001$) calculated for neurons across all sessions in monkey T. **(b)** Same as in a except for monkey M (123 neurons, mean $\Delta CSI = 0.05 \pm 0.001$, Wilcoxon signed rank test, $P < 0.0001$).

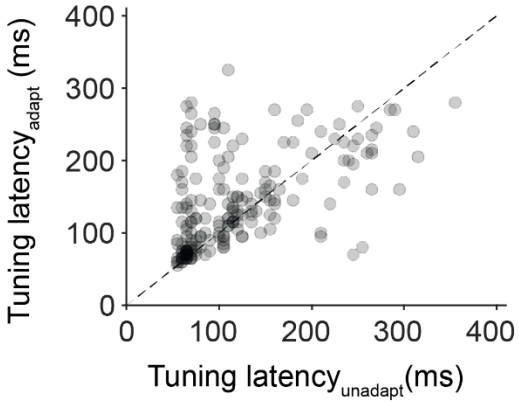

Supplementary Fig. 7 Cross-feature adaptation increases latency to peak tuning. Tuning latency (L) values (see Methods) for neurons significantly tuned under both conditions. An oriented grating was used as the adapter while tuning was examined for color stimuli. Each gray circle represents the tuning latency in both conditions for a single neuron. A significant increase in latency is observed post adaptation ($L_{unadapt} = 119 \pm 5$ ms, $L_{adapt} = 140 \pm 5$ ms; Wilcoxon signed rank test, $P < 0.0001$).

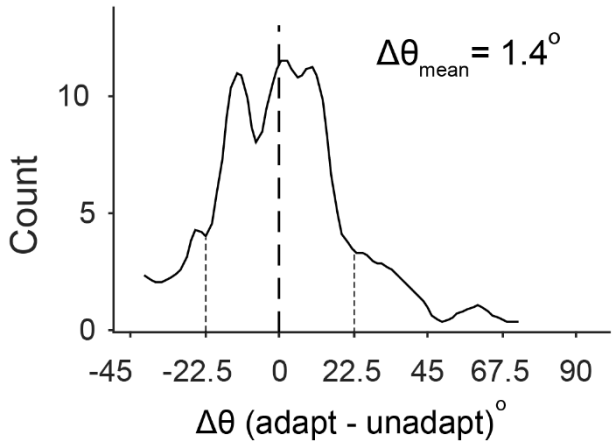

Supplementary Fig. 8 Modest changes in preferred color after cross-feature adaptation. Distribution of change in preferred color (Δθ) of neurons pooled across all sessions. Out of 343 neurons analyzed across both animals, only 18% showed changes in preferred color > 22.5°, i.e., the resolution of the color stimuli used in the experiments (16 equiluminant colors evenly distributed on the hue circle spanning 0 to 360°). Dotted vertical lines separate the distribution into regions greater or less than ±22.5° (resolution of the color stimuli in hue space, see Fig. 2a) and are included for visualization purposes.

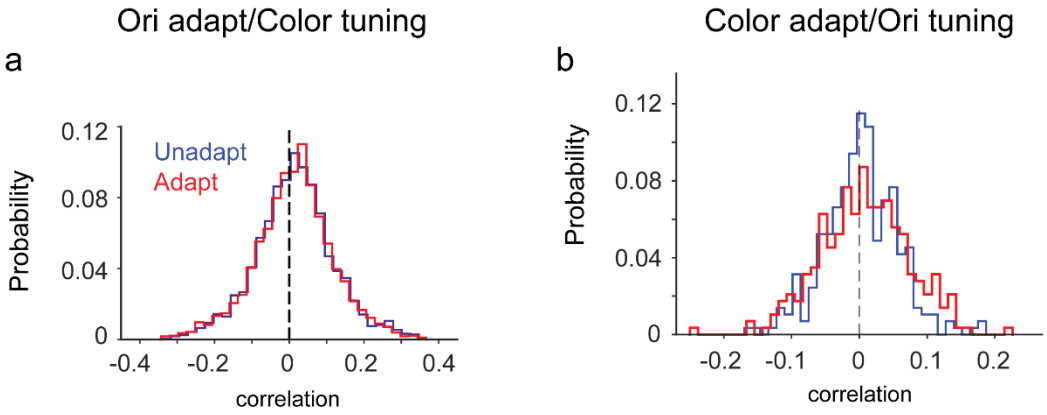

Supplementary Fig. 9 Distribution of pairwise correlations remain unchanged after cross feature adaptation (a) Distribution of pairwise noise correlations (n = 2817 pairs) in the unadapted (blue) and adapted condition (red) in the case of orientation adapt/color test. **(b)** Distribution of pairwise noise correlations (n = 288 pairs) before and after adaptation (color adapt/orientation test).

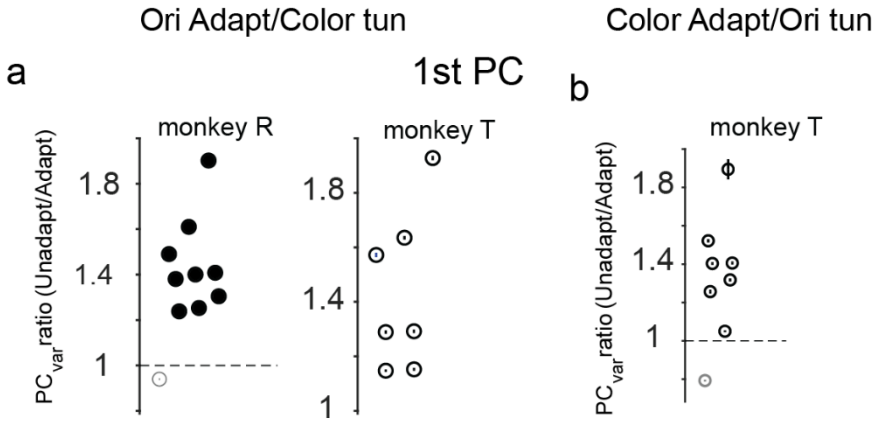

Supplementary Fig. 10 Higher variance in trial-by-trial population activity captured by the 1st principal component in unadapted versus adapted trials during passive fixation. Mean values of the ratio of variance in trial-by-trial population activity explained by the 1st principal component in unadapted and adapted conditions (orientation adapter/color test) for each individual session in monkey R (solid black circles) and monkey T (open black circles). Error bars were calculated by performing PCA analysis on sub-sampled trials in each condition. Lighter shaded circles represent sessions where the ratio is not significantly greater than 1 (Wilcoxon signed rank test, $P > 0.05$). **(b)** Same as in a except for color adapter and orientation test stimuli.

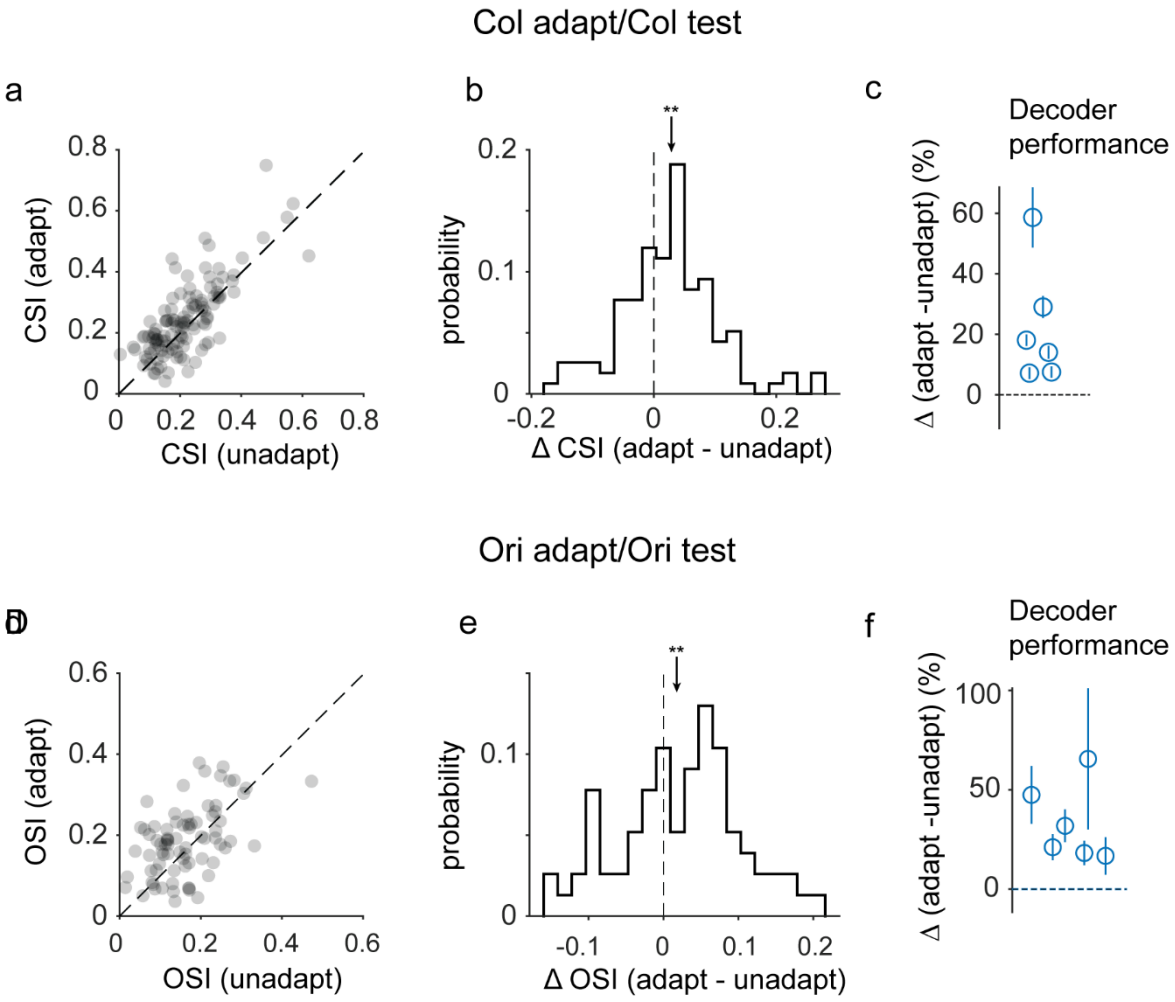

Supplementary Fig. 11 Iso-feature adaptation increases overall tuning strength and discriminability by de-correlating population responses to stimuli. **(a)** CSI values of color tuning in unadapt and adapt conditions for color adaptation. **(b)** Histogram of difference in CSI values (adapt-unadapt). Arrow represents mean change in CSI and asterisks denote $P < 0.01$ (Wilcoxon signed rank task). **(c)** Percentage change in decoder accuracy values (adapt - unadapt) for each session. Each unfilled circle represents a session and error bars (s.e.m) were calculated by running the decoder multiple times with a different set of training and test trials. **(d-f)** Same as in a-c except for when the test and adapting stimulus were oriented gratings.